

Development of a High-Flow Centrifugal Compressor Stage

KAWAKUBO Tomoki : Manager, Turbomachinery & Engine Technology Department, Product Development Center, Corporate Research & Development

UNNO Masaru : Manager, Computational & Mathematical Engineering Department, Research Laboratory, Corporate Research & Development

NUMAKURA Ryusuke : Doctor of Engineering, Manager, Turbomachinery & Engine Technology Department, Product Development Center, Corporate Research & Development

SHIMOHARA Naoto : Assistant Manager, Turbomachinery & Engine Technology Department, Product Development Center, Corporate Research & Development

KOTANI Koji : Manager, Engineering and Development Group, Engineering Department, Industrial Compressor Business Unit, General Headquarters of Industrial Machinery, IHI Rotating Machinery Engineering, Co., Ltd.

A turbo-compressor is a type of multi-stage centrifugal compressor that is often used in factories to boost or compress gaseous fluids. By making its overall size more compact than ever before, it is possible to reduce the initial costs associated with the installation of a new compressor. In order to realize a more compact compressor, the same amount of fluid must be processed in a smaller space; that is, a higher flow capacity will be required for each of the constituent compressor stages. However, squeezing fluid forcibly into a smaller space will result in a higher through-flow velocity and/or a more acute flow turning, which inevitably makes it difficult to maintain or improve the stage efficiency. Moreover, raising the height or reducing the thickness of the blades for the purpose of widening the cross-section of the passage may result in an increase in blade stress and/or a reduction in the blade's natural frequency. This report describes the efforts made to overcome the above-mentioned technical challenges that occurred in the development of a high-flow compressor stage that is intended to be applied in integrally-g geared turbo-compressors.

1. Introduction

A turbo-compressor is a type of multi-stage centrifugal compressor that is often used in factories to boost or compress gaseous fluids. Industrial compressors include various types of compressors such as, in addition to the turbo-compressor, a screw compressor and a reciprocating compressor. Power necessary to drive such compressors in a typical factory occupies a large portion of total power usage of the factory, so the energy saving of a high-pressure gas supply system including the compressors is strongly demanded⁽¹⁾. In addition, if the same specified flow rate of gas can be boosted/compressed by a smaller-sized compressor, the initial introduction cost of a compressor can be reduced. Accordingly, providing a more efficient and compact turbo-compressor results in a contribution to a reduction in the total cost related to boosting and compression in factories.

By increasing the flow capacity of each of stages constituting a turbo-compressor, the overall compressor size can be reduced. However, the increase in flow capacity generally involves an increase in the flow velocity of internal flow, thus easily causing increases in shock wave loss and friction loss. For this reason, it is desirable to make impeller blade and diffuser vane heights as high as possible and make blade and vane thicknesses as thin as possible. However, this causes ① an increase in stress, ② a reduction in stiffness, ③ a reduction in natural frequency, and so on in blades and vanes,

and therefore in order to ensure structural reliability, it is indispensable to appropriately set the blade and vane heights and the blade and vane thicknesses. Further, in the case of an integrally-g geared turbo-compressor, even when the flow capacities of the impeller and diffuser can be successfully increased, correspondingly increasing the outermost diameter of the scroll easily causes the interference between the scroll and other parts, and consequently the adjustment of overall layout may become difficult.

In order to increase the flow capacity of a turbo-compressor, how we can overcome the above-described technical challenges is the key. This report describes the efforts made to overcome the technical challenges that occurred in the development of a high-flow compressor stage intended to be applied in integrally-g geared turbo-compressor.

2. Aerodynamic and structural features of turbo-compressor

Each stage of a turbo-compressor is configured to include mainly an impeller as rotating blades, a diffuser as stationary vanes, and inter-stage flow passages for connecting between adjacent stages. Energy is transmitted from a drive source to working fluid via the impeller, and part of the energy is converted to pressure energy in the impeller. Part of the remaining kinetic energy is converted to pressure energy in the diffuser, and the working fluid is sent to the next stage. A turbo-compressor can be roughly divided into two types in

terms of structure (see Fig. 1). One is a single-shaft multi-stage type as illustrated in Fig. 1-(a), in which multiple impellers are successively assembled to a single shaft, facing in the same direction, and supported by bearings at both ends of the shaft. When the rotor speed of the compressor is higher than that of a driving motor, a speed-increasing gear is used. The other one is an integrally-gear type as illustrated in Fig. 1-(b), in which around a bull gear shaft directly connected to a driving motor, multiple pinion shafts are arranged, and one or two impellers are assembled to each of the pinion shafts, facing to a shaft end side. The pinion shafts are acceleratedly driven by a bull gear, and in an overhanging manner, supported by bearings arranged interposing a gear engaging part.

Figure 2 illustrates examples of a centrifugal compressor impeller. In the case of the former single-shaft multi-stage type (see Fig. 1-(a)), a closed type (see Fig. 2-(a)) is often used as the impellers, and an axisymmetric return flow passage connects adjacent stages. Because the rotor speed of the closed type impeller cannot be increased so much due to the strength reason, a pressure ratio per stage is required to be set to be relatively low. However, by stacking many stages, the total pressure ratio can be increased.

On the other hand, in the case of the latter integrally-gear type (see Fig. 1-(b)), a stage is connected to the next stage through an intercooler via a non-axisymmetric scroll.

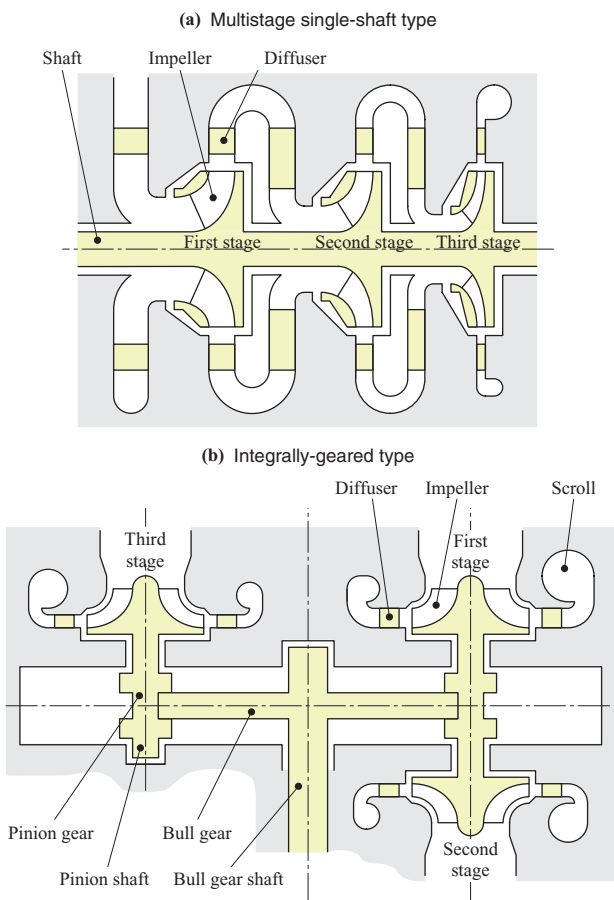


Fig. 1 Structure of a turbo-compressor

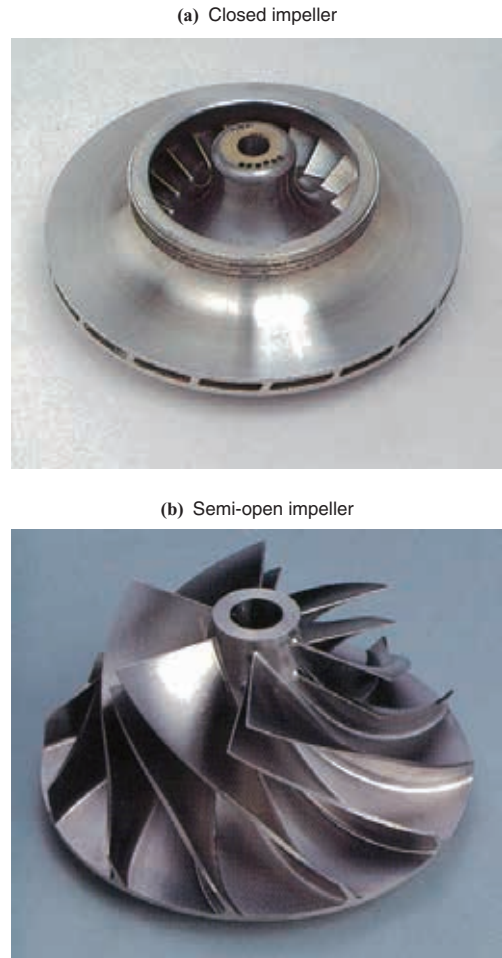


Fig. 2 Example of centrifugal compressor impellers

impellers, a semi-open type (see Fig. 2-(b)) is often used, which is suitable for increasing flow capacity and pressure ratio.

The multi-stage turbo-compressor is such that working fluid is compressed and gradually decreased in volume every time it passes through a stage, so a larger flow coefficient applies to front stages, whereas a smaller flow coefficient applies to rear stages. Note that a flow coefficient ϕ is a dimensionless number defined by Equation (1) below.

$$\phi = \frac{G}{\rho_{01} D_2^2 u_2} \dots\dots\dots(1)$$

Here, G represents a mass flow rate, ρ_{01} stagnation density at the inlet of a stage, D_2 the impeller tip diameter, and u_2 the impeller tip speed. The flow coefficient serves as one of indicators representing the capacity of the stage.

On the other hand, the boosting capability of the stage (stage loading) is evaluated by a pressure coefficient μ_y , given by Equation (2) below.

$$\mu_y = \frac{\Delta h_{ad}}{u_2^2} \dots\dots\dots(2)$$

Here, Δh_{ad} represents the stage adiabatic enthalpy rise, and under the assumption of perfect gas, can be obtained by Equation (3) below.

$$\Delta h_{ad} = C_p T_{01} \{P_r^{(\gamma-1)/\gamma} - 1\} \quad \dots\dots\dots(3)$$

Here, P_r represents the pressure ratio (total pressure ratio) between the inlet and outlet of the stage, T_{01} the total temperature at the inlet of the stage, and C_p and γ the isobaric specific heat and specific heat ratio of the working fluid. Since both of the flow coefficient and the pressure coefficient include the impeller tip speed in the denominators, it can be said that a semi-open impeller, more likely to have higher tip speed, is suitable for increasing flow capacity and pressure ratio.

Replacing the numerator of Equation (2) with the actual stage enthalpy rise Δh gives a work coefficient μ_0 expressed by Equation (4) below.

$$\mu_0 = \frac{\Delta h}{u_2^2} \quad \dots\dots\dots(4)$$

The ratio between the pressure coefficient and the work coefficient is called adiabatic efficiency η_{ad} given by Equation (5) below.

$$\eta_{ad} = \frac{\mu_y}{\mu_0} \quad \dots\dots\dots(5)$$

Specific speed N_s defined by Equation (6) below has an optimum range for each compressor type, and in the case of a centrifugal compressor, a range of approximately 0.1 to 0.12 is optimum⁽²⁾.

$$N_s = n \frac{\sqrt{G / \rho_{01}}}{\Delta h_{ad}^{3/4}} = \frac{\sqrt{\phi}}{\pi \mu_y^{3/4}} \quad \dots\dots\dots(6)$$

Here, n represents the rotor speed of a compressor. Originally, the specific speed is a dimensionless number for evaluating how much the rotation number falls outside the optimum range. In the case of a centrifugal compressor, the pressure coefficient is set to a narrow range of approximately 0.45 to 0.65, and tends to moderately decrease as the flow coefficient increases. Accordingly, the specific speed expressed by the combination of these two dimensionless numbers can be considered as an indicator representing the capacity of the compressor as with the flow coefficient.

Finally, a peripheral Mach number M_{u2} is a dimensionless number representing the rotor speed of the impeller, and defined by Equation (7) below.

$$M_{u2} = \frac{u_2}{a_{01}} \quad \dots\dots\dots(7)$$

Here, a_{01} represents sound velocity defined in a stagnation state at the inlet of the stage. In the case of perfect gas, the pressure ratio P_r can be expressed by Equation (8) below.

$$P_r = \{1 + (\gamma - 1) \mu_y M_{u2}^2\}^{\gamma/(\gamma-1)} \quad \dots\dots\dots(8)$$

From Equation (8), it turns out that in order to increase the pressure ratio of a stage (in order to increase the head), it is indispensable to increase tip speed or loading.

3. Development method

3.1 Approach to increasing flow capacity

The capacity of a turbo-compressor roughly refers to the volume of air or gas boosted/compressed by the compressor per unit time, i.e., to the flow rate of the air or the gas. Also, an increase in the flow capacity of a compressor means that a compressor of the same external size can handle a higher flow rate, and increasing flow capacity allows a smaller compressor to handle the same flow rate, thus making it possible to decrease an external size or achieving compactification. That is, aerodynamically, an increase in flow capacity \equiv a decrease in external size \equiv compactification.

Figure 3 schematically illustrates two different approaches to an increase in flow capacity or compactification. Three main elements constituting each stage of an integrally-geared turbo-compressor are an impeller as rotating blades, a diffuser as stationary vanes, and a scroll for collecting compressed gas to send it through a flow passage to the next stage. Here, we consider an increase in flow capacity by decreasing the external size of a base compressor without changing a flow rate itself.

Approach ① (see **Fig. 3-(a)**) is one adapted to downsize only the scroll that is an element occupying a space on the outermost circumferential side among the above three elements. An advantage in this case is that the number of new structural risks is small because it is not necessary to change the rotor speed of the impeller. On the other hand,

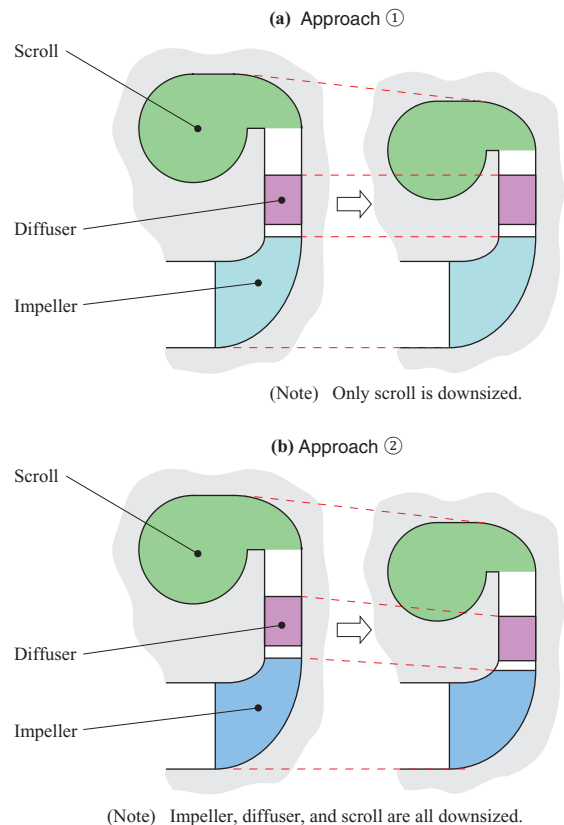


Fig. 3 Approaches to realizing a higher flow capacity and greater compactness

since compactification depends on only the scroll, there is a disadvantage that an aerodynamic burden is concentrated on the scroll, and therefore it is not easy to achieve high performance (there is less margin for the trade-off among the elements).

On the other hand, Approach ② (see Fig. 3-(b)) is one adapted to downsize all of the impeller, diffuser, and scroll. Of course, since all the elements are downsized, the tradeoff is flexibly controllable, and high performance can be easily kept. However, in order to obtain the same pressure ratio as that of the base compressor, the rotor speed must be increased, and consequently new risks may occur, such as an increase in impeller stress and the vibration of impeller blades and/or diffuser vanes.

In general terms, Approach ② seems to have a larger margin for improving efficiency. However, unless an improvement in the aerodynamic performance of the impeller and diffuser and reductions in the risks of strength and blade/vane vibration can be achieved, the advantage may be limited as with Approach ①.

In this development, we have attempted the compactification based on Approach ① firstly. With compactifying an existing base compressor stage by 10% as a target, an aerodynamic study was performed on the following two cases, i.e., the case where a base scroll was simply scaled down by 10%, and the case where the outermost diameter of the scroll was decreased by 10% and the configuration of a scroll flow passage was adjusted so as to further suppress a reduction in efficiency. As a result of the study using a one-dimensional loss model, in the former case, a reduction in efficiency was estimated to be 0.8 points, whereas in the latter case, the reduction was estimated to be only 0.4 points. On the basis of the above results, the latter scroll was actually produced and the component test with it was conducted in order to compare the overall compressor performance with the base one, as shown in Fig. 4. As was estimated, it was confirmed that a reduction in efficiency associated with the compactification of the scroll was approximately 0.5 points or less.

From the above study results, it was confirmed that although the compactification based on Approach ① was effective, in order to further increase efficiency and pressure ratio simultaneously with compactification, a new target was set again, and the development of a compressor stage based on Approach ② was started. This report mainly describes the development based on Approach ②. Note that although Fig. 3 illustrates as if the compressor stage is wholly decreased in size, in the actual development, the impeller tip diameter and the outermost diameter were kept unchanged and the flow rate was increased in accordance with the similarity law. Also, in the actual development, for the scroll, the configuration of the existing base one is directly used.

3.2 Technical challenges associated with increase in flow capacity

To increase flow capacity, various factors of performance reduction (efficiency reduction and operating range reduction) associated with the narrowing must be suppressed or relieved in terms of aerodynamics. Figure 5 illustrates the comparison

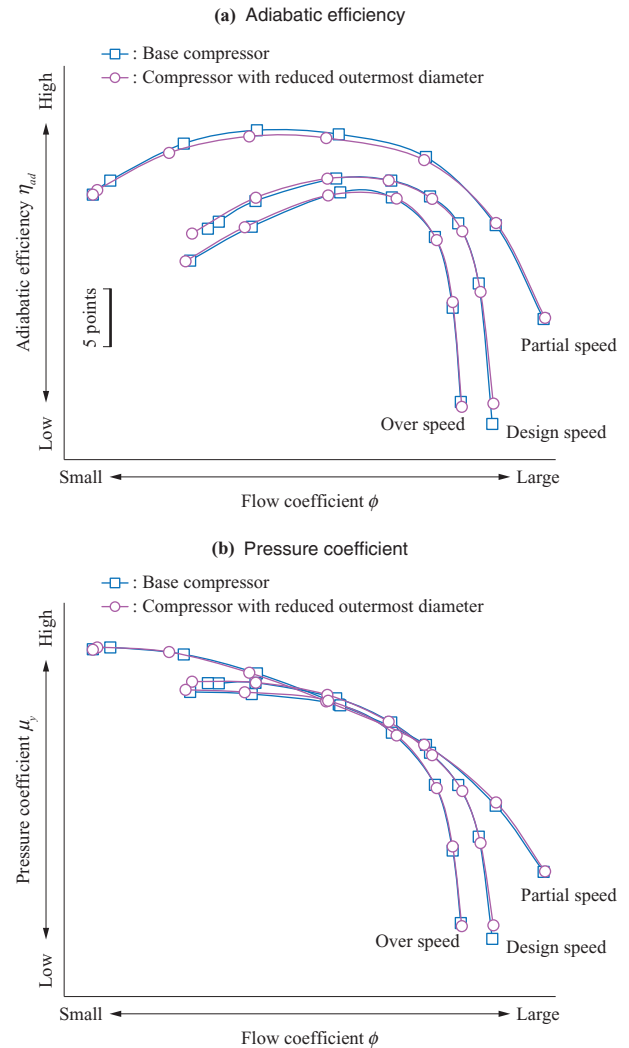


Fig. 4 Overall performance of the compressor

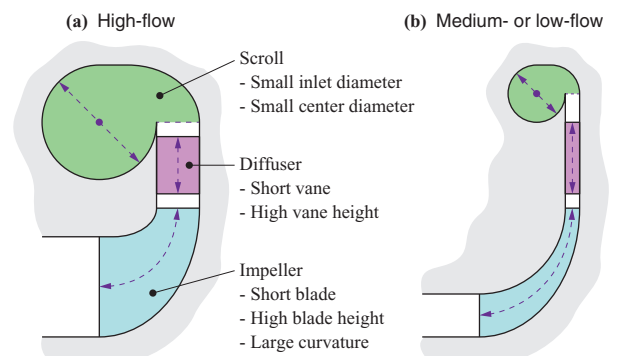


Fig. 5 Comparison of high-flow and medium- or low-flow compressors

between a high-flow compressor and a medium- or low-flow compressor. For example, ① reductions in shock wave loss and friction loss associated with an increase in flow velocity, ② reductions in bend loss and separation loss associated with flow passage layout in a narrow space, ③ suppression of the effect of a non-axisymmetric static pressure distribution due to a scroll, ④ suppression of the effect of inlet distortion from the upstream side (circumferential distortion of inflow),

and so on can be cited.

On the other hand, concerning the strength and blade/vane vibration, there are the following technical challenges. In order to increase a flow rate, it is desirable to make impeller blade and diffuser vane heights as high as possible, and to make blade and vane thicknesses as thin as possible. However, it is necessary to simultaneously suppress an increase in centrifugal stress occurring in impeller blades or a disk and ensure the buckling strength of diffuser vanes. In addition, it is also necessary to prevent reductions in the natural frequencies of impeller blades and diffuser vanes and thereby sufficiently ensure a detuned range. Further, it is necessary to suppress the interference between the rotating blades and the stationary vanes so as not to intensify the excitation for the impeller vibration.

3.3 Design analysis approach

In this development, Computational Fluid Dynamics (CFD) simulation was extensively applied to the aerodynamic design of the impeller and the diffuser. The CFD solver used was a compressible, viscous, and finite difference Navier-Stokes solver developed in-house for a turbomachinery cascade. The Chakravarthy-Osher TVD scheme was used for the convective term and the Spalart-Allmaras model was used as the turbulence model. As boundary conditions, total pressure, total temperature, and flow angle were fixed at the inlet boundary, and at the outlet boundary, static pressure was fixed. In addition, the mixing plane model was used to connect the rotor blade and stator vane regions. For this reason, steady state analysis was employed, in which one of each of the impeller passages and the diffuser passages was modeled, and periodic boundary conditions were applied to the circumferential boundaries. In addition, since in this development, the configuration of the existing base scroll was directly used, without performing the CFD analysis on the scroll portion, a change in scroll performance associated with a change in flow at the outlet of the diffuser was estimated using the one-dimensional loss model.

As a Finite Element Method (FEM) solver necessary for stress analysis, natural frequency analysis, and buckling analysis, general-purpose software ANSYS or Nastran was used. To analyze the impeller, a bladed disk model in which one pitch between adjacent blades is modeled was used, and a cyclic symmetry condition was applied to the circumferential boundary. On the other hand, to analyze the diffuser, only one vane was modeled, and a fixed condition was applied to the root of the vane.

4. Aerodynamic design and structural design

4.1 Design specifications

Table 1 lists design specifications as the development targets of the high-flow compressor in comparison with the base compressor. An increase in flow capacity by 27% and an increase in head by means of increased tip speed by 36% as compared with the base compressor were set as the targets. Also, we set the adiabatic efficiency, the surge margin, and other specifications to be equivalent to the base values or higher as the targets. In Approach ① described above, the outermost diameter was reduced by 10%, which corresponds to an increase in flow capacity by 23%. At the same time, a reduction in efficiency by approximately 0.5 points was observed, so the above efficiency target means that we aimed at an improvement in efficiency exceeding the base compressor by approximately 0.5 points.

Figure 6 illustrates the comparison between the above target performance and the performance of existing centrifugal compressors and mixed flow compressors picked up from literatures and other such material. The base compressor itself is already at a high level in specific speed and pressure ratio as a centrifugal compressor. The high-flow compressor is set to have target performance exceeding that of the base compressor, and falls within a range where not many previous centrifugal compressors stay.

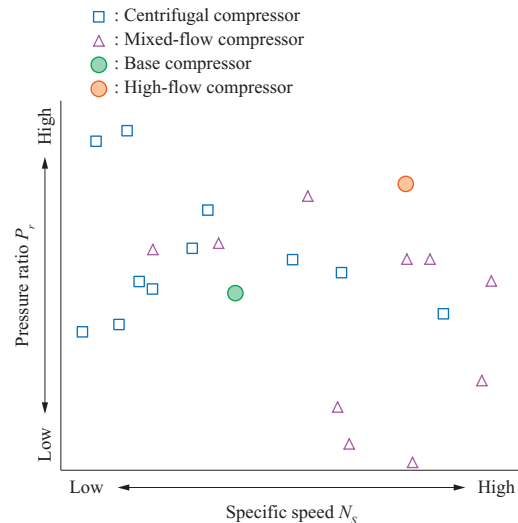


Fig. 6 Trends in high-flow compressor stages and target performance

Table 1 Design specifications for the high-flow compressor stage

Item	Symbol	Unit	Base compressor	High-flow compressor
Impeller tip Mach number	M_{t2}	—	(Base)	+19%
Flow coefficient	ϕ	—	(Base)	+27%
Pressure coefficient	μ_y	—	(Base)	(Equivalent)
Adiabatic efficiency	η_{ad}	—	(Base)	(Equivalent)
Surge margin	SM	%	(Base)	(Equivalent)
Head margin	HM	%	(Base)	(Equivalent)

4.2 Impeller design

The impeller as a rotor is the aerodynamically most important element for transmitting the power of the rotary shaft to fluid. Because the impeller is a rotating body, it gives rise to stress due to the centrifugal force, as well as receives a periodic aerodynamic force from stationary structures such as the diffuser. Accordingly, when designing the impeller, a well-balanced trade-off between aerodynamic design and structural design is very important.

Figure 7 illustrates a detailed design flow of the impeller. The design of the impeller is performed in the order of ① setting of meridional shape (see **Fig. 7-(a)**), ② setting of blade angle distribution **(-b)**, ③ setting of blade thickness distribution **(-c)**, and ④ setting of disk geometry **(-d)**. Among these configuration setting steps, the setting of the meridional shape and blade angle distribution is strongly related to performance parameters such as a flow rate, pressure ratio, efficiency, and surge margin. For this reason, designer's experience and intuition and geometry change based on flow pattern observation are quite effective. For the aerodynamic evaluation of them, the CFD analysis is used. However, it takes a relatively long time to conduct the CFD analysis, and also human decision is required for evaluations such as the evaluation of convergence and stability and the evaluation of a flow pattern to be improved.

On the other hand, the setting of the blade thickness distribution and the disk shape is strongly related to main strength items such as the stress and the natural frequency, and these main items can be automatically evaluated to some extent. For these strength evaluations, the FEM analysis is used, and as compared with the CFD analysis, the FEM analysis takes a remarkably shorter time and can stably obtain a solution without any trouble. Accordingly, we decided to accelerate the entire design loop by performing the former mainly on the basis of designer's experience and decision in a conventional manner, and automatically optimizing the latter with the aid of an optimization tool.

Evaluation parameters used for the optimization are the maximum stress, a detuned range, and the maximum blade thickness. Note that the detuned range refers to a ratio of an operating range where an excitation frequency (the number of diffuser vanes $Z_v \times$ rotor speed n) and an impeller natural frequency are detuned from each other at a detuning rate⁽³⁾ having a predetermined value or more to an assumed operating range (rotor speed range). As geometric parameters, the meridional shape, blade angle distribution, the number of nodal diameters, blade root fillet radius, and disk bore shape were fixed, and blade thickness distribution, splitter blade leading edge position and shape, and disk back shape were changed to maximize the detuned range. The reason to use

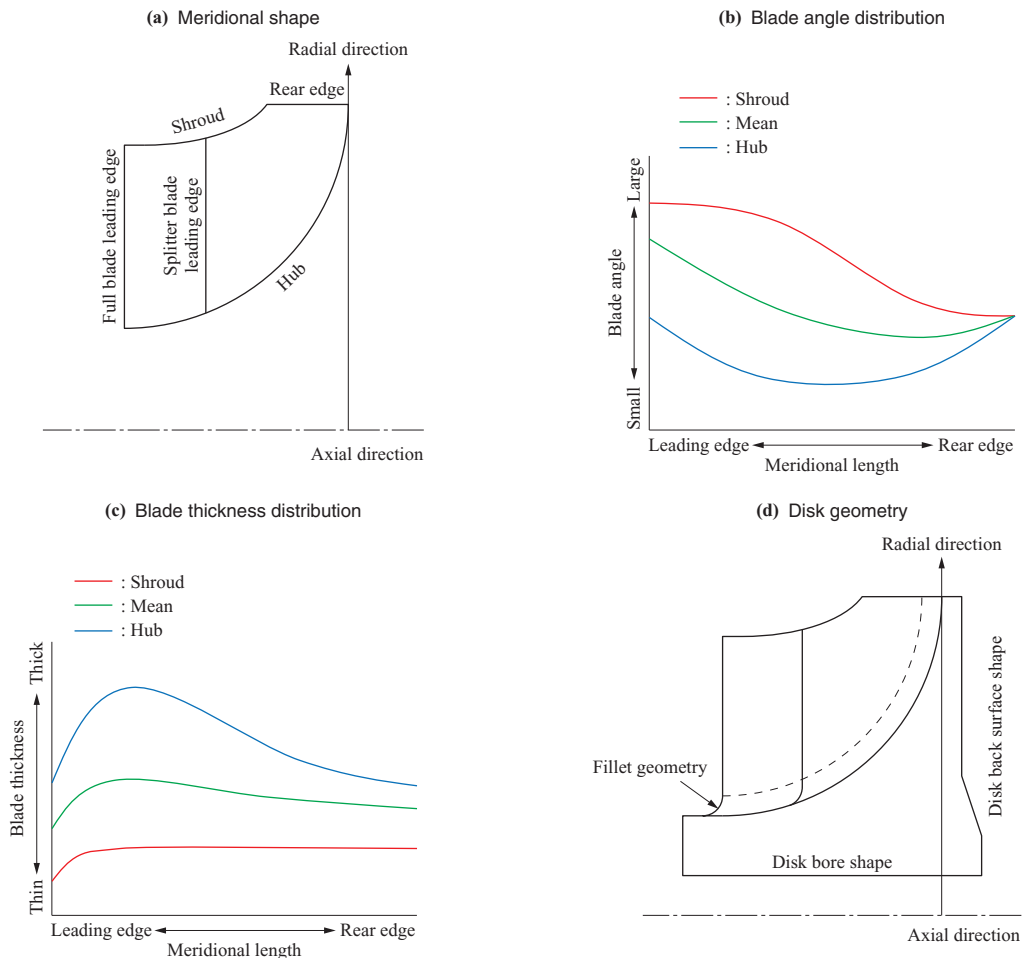


Fig. 7 Detained design process for the impeller

the maximum blade thickness as one of the evaluation parameters is because if this is not included, in order to increase the detuned range, the blade thickness infinitely increases. Isight was used for the optimization, and as an optimization algorithm, a genetic algorithm was used.

Figure 8 illustrates optimization results for the impeller configuration. As the final solution, selected was one where the detuned range was wide and the maximum stress was low. The maximum stress is correlated to the natural frequency to some extent, and therefore tends to decrease with increasing the detuned range.

Table 2 lists the differences in efficiency and detuned range among the base impeller, typical impellers (Impeller A and Impeller B) in the intermediate stage of design, and the finally selected impeller (Impeller C). As listed in **Table 1**, since the base impeller is not assumed to be used in a high tip speed region originally, if the high tip speed region is included in the assumed operating range, the detuned range becomes very narrow. In such a case, even if two alternative diffusers having different numbers of vanes are prepared, a large operating range where detuning is impossible remains. In the case of Impeller A where flow capacity and tip speed were increased relative to the base impeller with a focus only on strength, the detuned range increases, whereas the efficiency significantly decreases. On the other hand, in the case of Impeller B the aerodynamic performance of which was intentionally improved, the efficiency is improved simultaneously with the expansion of the detuned range. Further, in the case of Impeller C where strength was optimized, both the efficiency and the detuned range are significantly improved as compared with the base impeller. In the case of Impeller C, by preparing alternative diffusers having different numbers of vanes, complete detuning can be achieved.

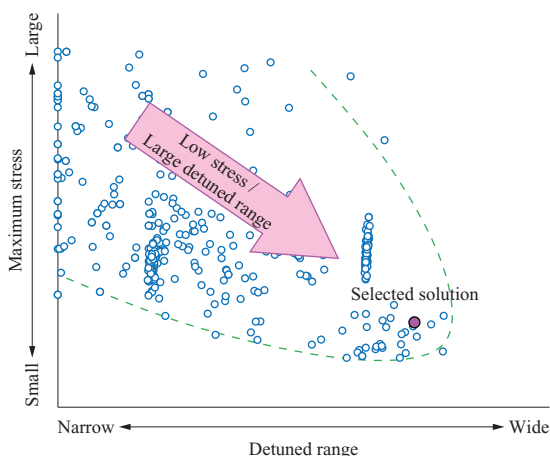


Fig. 8 Optimization results for the impeller configuration

Table 2 Impeller efficiency and detuned range

Item	Base impeller	Impeller A	Impeller B	Impeller C
Impeller efficiency	(Base)	-4.1 pts	+1.6 pts	+2.0 pts
Detuned range	(Base)	+13 pts	+42 pts	+49 pts

(Note) pts : points

For the purpose of analyzing the difference in efficiency between Impellers A and B, **Fig. 9** illustrates streamlines in the impellers. In the case of Impeller A (see **Fig. 9-(a)**), streamlines are tangled to form a stagnant region on the outlet side of the impeller. This is because a blade-to-blade loading is too high, and therefore high loss fluid caused by clearance leakage and secondary flows from the hub surface and the suction surface cannot flow down but is accumulated. In addition, part of fluid having flowed out toward the downstream side of the impeller flows back and is again taken in this region. Further, part of stagnant fluid in a passage on the splitter blade pressure side spills over from a splitter blade leading edge and is again trapped in a stagnant region in an adjacent passage on the suction side. In order to improve these problems, in Impeller B (see **Fig. 9-(b)**), by increasing the number of blades and extending splitter blades toward the upstream side, the blade-to-blade loading was totally reduced. As a result, it turns out that the clearance leakage flow and the secondary flows smoothly join a flow toward the impeller outlet without accumulating too much. It can be thought that the above-described improvement in flow pattern resulted in the improvement in impeller efficiency.

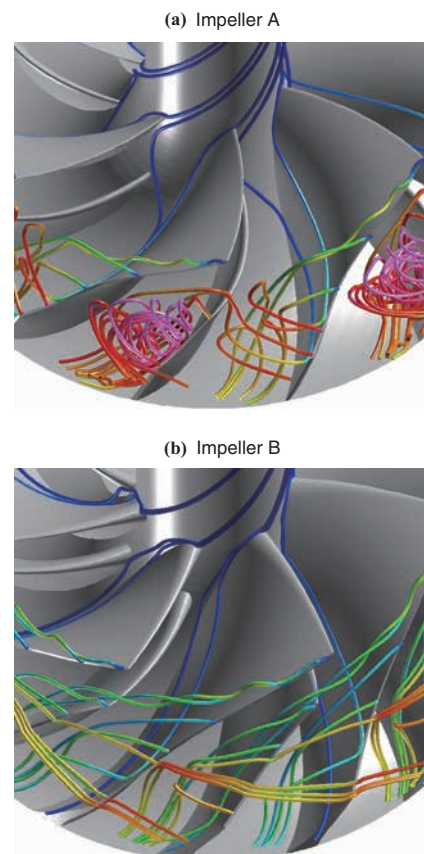


Fig. 9 Streamlines in the impeller

Next, the difference in efficiency between Impellers B and C will be examined. **Figure 10** illustrates the distribution of the relative Mach number at the impeller shroud section. In the case of the base impeller illustrated for reference, calculation result at a flow rate corresponding to the design flow coefficient of the base compressor is illustrated. In the cases of Impellers B (see **Fig. 10-(b)**) and C (see **-(c)**), with increasing the design flow coefficient, high Mach number regions are widened as compared with the base impeller. As a result, in Impeller B, a strong shock wave occurs on the suction surface of a full blade. On the other hand, in Impeller C, the strength of a shock wave is reduced by adjusting the curvature of blades near the impeller inlet. This may be the reason for the slight increase in the efficiency of Impeller C as compared with Impeller B. Such an improvement in flow field characteristics greatly depends on the adjustment of the blade angle distribution based on designer's skill and experience. Accordingly, rather than depending on the optimization algorithm, an experienced designer can more quickly reach an expected solution just by designing manually.

4.3 Diffuser design

The diffuser is an element for converting kinetic energy applied to fluid by the impeller to pressure energy. This compressor employs a vaned diffuser which is a kind of airfoil diffuser. Since the diffuser is a set of stationary vanes, there is no stress due to rotation. However, it is periodically affected by variable fluid force from the impeller in rotation, so it is necessary to detune the vane natural frequency from the excitation frequencies. Also, when a compressive load is put in an assembled state, buckling should be prevented. From the above, the appropriate trade-off between aerodynamics and structure becomes important for the diffuser as well, although the importance is not so high as for the impeller.

Figure 11 illustrates streamlines near diffuser shrouds (streamlines in the diffuser of the base compressor and those in the diffuser of the high-flow compressor). In the base diffuser, corner separation occurs on the shroud/suction-side corners to form a stagnant region. Flow leaving from a separation region reaches an adjacent diffuser vane, and is

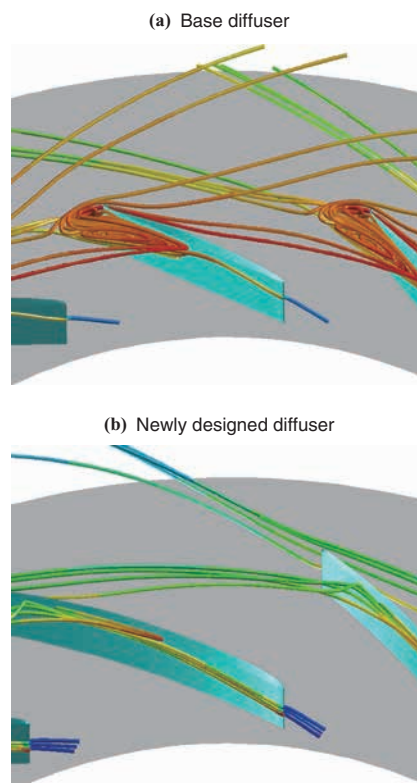


Fig. 11 Streamlines near the diffuser shroud

trapped in a stagnant region there. In addition, on the downstream side of the diffuser, backflow occurs, and is also trapped in a stagnant region caused by corner separation. For the base compressor, such an operation state is an overspeed state, which was not assumed when the base compressor was designed (see **Table 1**). For this reason, the diffuser is burdened with an overload, thus causing such separation and backflow. On the other hand, in the diffuser designed for the high-flow compressor, such secondary flows on the shroud side are suppressed, and remarkable corner separation is not observed, resulting in a good flow pattern.

Next, in order to increase structural reliability, the vanes of

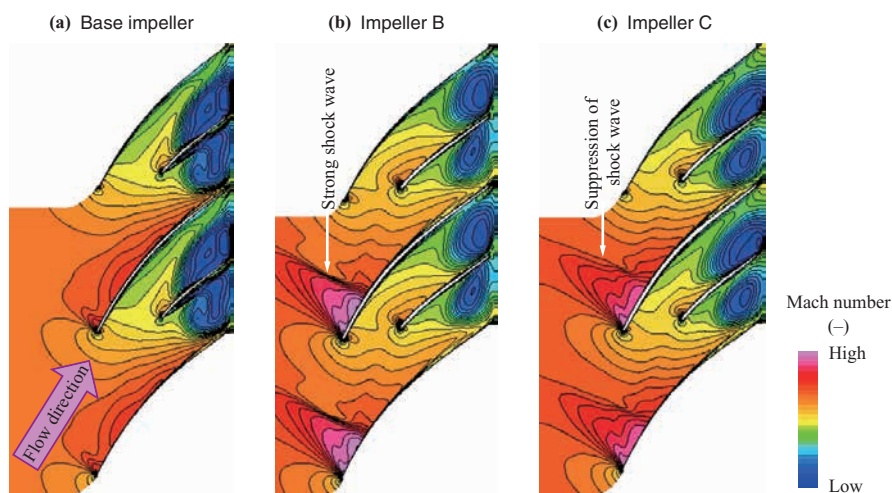


Fig. 10 Distribution of the relative Mach number of the impeller shroud section

the newly designed diffuser were thickened. **Figure 12** illustrates Mach number distributions on the diffuser shroud side (CFD analysis result) before and after the thickening. By thickening the vanes, flow velocity on the suction side increases, and the thickness of the boundary layer increases toward the trailing edge. In addition, a reduction in efficiency associated with the vane-thickening is as relatively small as 0.4 points. The thickening made it possible to double the primary natural frequency of the diffuser vane and increase the Euler buckling load approximately 7 times, and hence the reliability of the diffuser could be increased.

In the thicker vane diffuser, the vanes bulge toward the inner side to increase a blockage, and thereby circumferential pressure disturbance on the upstream side is also increased. Such a pressure disturbance results in an increase in exciting force to the impeller, so an increase in blade vibration amplitude at the time of resonance may be a concern. Basically, since the optimization design of the impeller significantly increased the detuned range as described above, when the thick vane diffuser is applied to actual products, the possibility of occurrence of the resonant state is extremely low. However, as will be described in **Chapter 5**, it was confirmed in the component test that a blade vibration

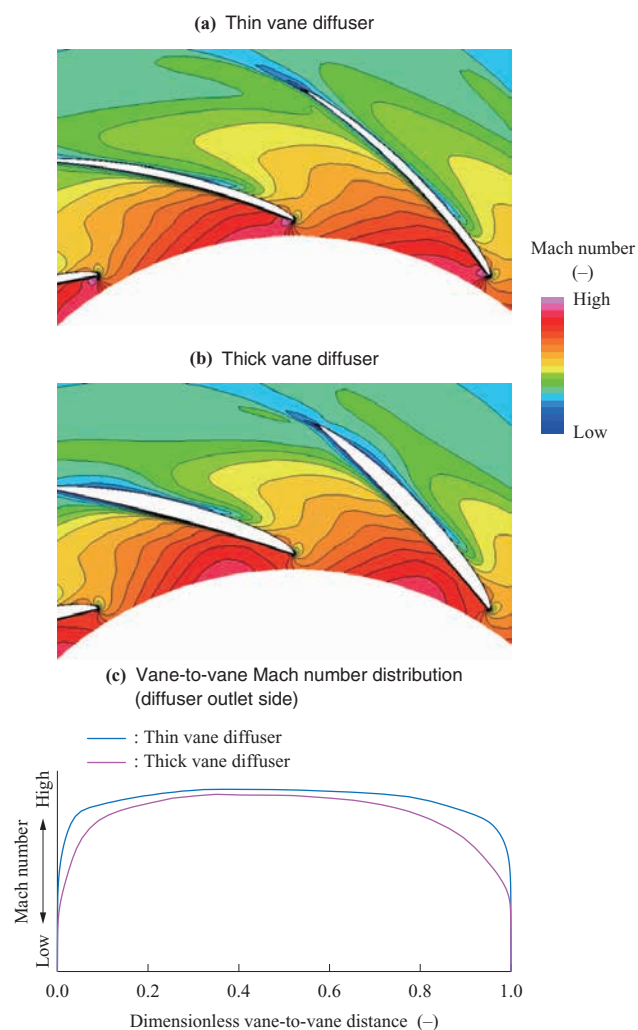


Fig. 12 Mach number distribution at the diffuser shroud section

response is sufficiently low.

5. Component test

5.1 Aerodynamic performance test

In order to check the aerodynamic performance of the newly designed high-flow compressor, test pieces of the impeller, diffuser, scroll, and so on for performance test were prepared, and assembled in a compressor test rig to measure overall performance. **Figure 13** illustrates the high-flow impeller test piece used for the test. For the test, an inverter motor-driven rotating test rig with a speed increasing gear was used. A compressor flow rate was adjusted using a back pressure adjustment valve on the downstream side of the compressor. Measurement items were total pressure, static pressure, and total temperature at the inlet and outlet of the compressor, a mass flow rate, rotor speed, atmospheric pressure, and atmospheric temperature. The total pressure, static pressure, and temperature were measured using a total pressure tube of Kiel-type, static pressure holes provided in the suction and discharge pipes, and a thermocouple of stagnation-type or sheath type, respectively. The mass flow rate and the rotor speed were measured by an orifice meter and a torque meter, respectively. A surge point (the stable operation limit point of the compressor) was comprehensively determined from a waveform of a high response semiconductor pressure sensor installed in the suction pipe, surging sound, and other factors.

Figure 14 illustrates the measurement results (the characteristic curves of adiabatic efficiency **(-a)** and pressure coefficient **(-b)** against a flow coefficient) of the overall performance of the centrifugal compressor at the design tip speed. The characteristic curves of the compressor sufficiently exceed the target performance values, and the increases in flow capacity and pressure ratio are achieved exceeding the initial target values (when actually applying the compressor to products, the flow rate and the pressure ratio are adjusted for each application by the shroud cut and the tip diameter cut with this test configuration as a reference configuration, so a slight increase in configuration is not a problem). The efficiency also exceeds the target value, and the peak efficiency is improved by 1 point or more relative to



Fig. 13 High-flow impeller used as a test piece

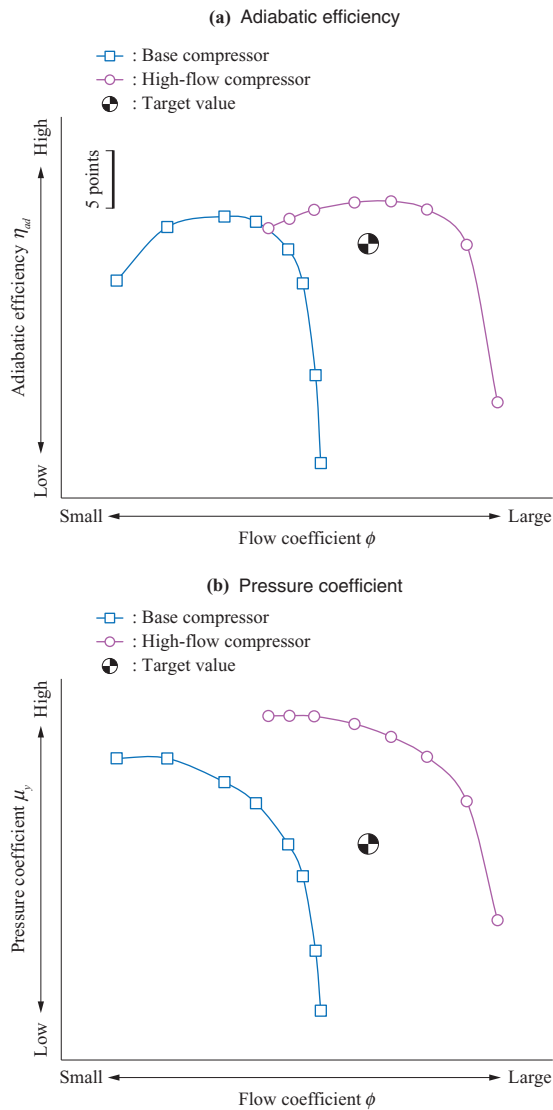


Fig. 14 Measurement results for an evaluation of the compressor's overall performance

the base compressor. In addition, the pressure coefficient at the peak efficiency point is also increased. Further, the width from the peak efficiency point to the surge point is also significantly expanded.

Table 3 lists the results of the aerodynamic rig test at the design tip speed and at a partial tip speed. High performance is achieved, in which any item exceeds a corresponding target

Table 3 Results of the aerodynamic rig test

(a) Design tip speed				
Item	Symbol	Unit	Target specification	High-flow compressor
Flow coefficient	ϕ	—	(Base)	+10%
Pressure coefficient	μ_y	—	(Base)	+10%
Adiabatic efficiency	η_{ad}	—	(Base)	+0.9 pts
Surge margin	SM	%	(Base)	± 0.0 pts
Head margin	HM	%	(Base)	+1.0 pts

(b) Partial tip speed				
Item	Symbol	Unit	Target specification	High-flow compressor
Flow coefficient	ϕ	—	(Base)	+1%
Pressure coefficient	μ_y	—	(Base)	+2%
Adiabatic efficiency	η_{ad}	—	(Base)	+1.2 pts
Surge margin	SM	%	(Base)	± 0.0 pts

(Note) pts : points

value, and the validity of the aerodynamic design approach toward a higher flow capacity was confirmed.

5.2 Blade vibration test

After the aerodynamic performance test, a test for checking a blade vibration response was performed. As the blade vibration measurement, both of strain gauge measurement and non-intrusive stress measurement were performed. The measurement was performed with diffuser vanes on the downstream side of the impeller, Variable Inlet Guide Vanes (VIGV) on the upstream side of the impeller, and the combination of both as excitation sources. The VIGV is such that the stagger angle (an angle formed between the axial direction and the centerline of the vane) is variable, and can be varied from 0 degrees (fully opened) to 90 degrees (fully closed). Under the presence of the VIGV, it is difficult to take a signal out of the strain gauge in terms of layout, so the measurement was performed only by the non-intrusive stress measurement. Although the rotating test rig was basically the same as that used for the aerodynamic performance test described in the previous section, black zinc plating was partially applied on the pinion shaft and sharp rotation signals were obtained by an optical sensor.

Before the blade vibration test, hammering-based natural frequency measurement was performed on both of the base impeller and the high-flow impeller. The results of the measurement agreed well with the results of the preceding FEM analysis, and the expansion of the detuned range of the high-flow impeller was confirmed.

Figure 15 illustrates the measurement results of impeller blade's vibration responses in the base compressor and the high-flow compressor. In **Fig. 15**, the size of a circle refers to the maximum initiation stress value converted from an amplitude measurement value using the FEM analysis results. Under the presence of the VIGV, the response changes depending on the opening angle of the VIGV. Also, even at the same VIGV opening angle, a response differs depending on a load condition (choke side, near peak efficiency point, surge side, and so on). In **Fig. 15**, the comparisons are made under conditions (VIGV opening angle and load condition) maximizing the vibration response in each of the compressors. In the case of the base impeller, at excitation order corresponding to the number of diffuser vanes, a clear response is observed (though the value of the response is sufficiently low with respect to the fatigue strength of the impeller). In the case of the high-flow

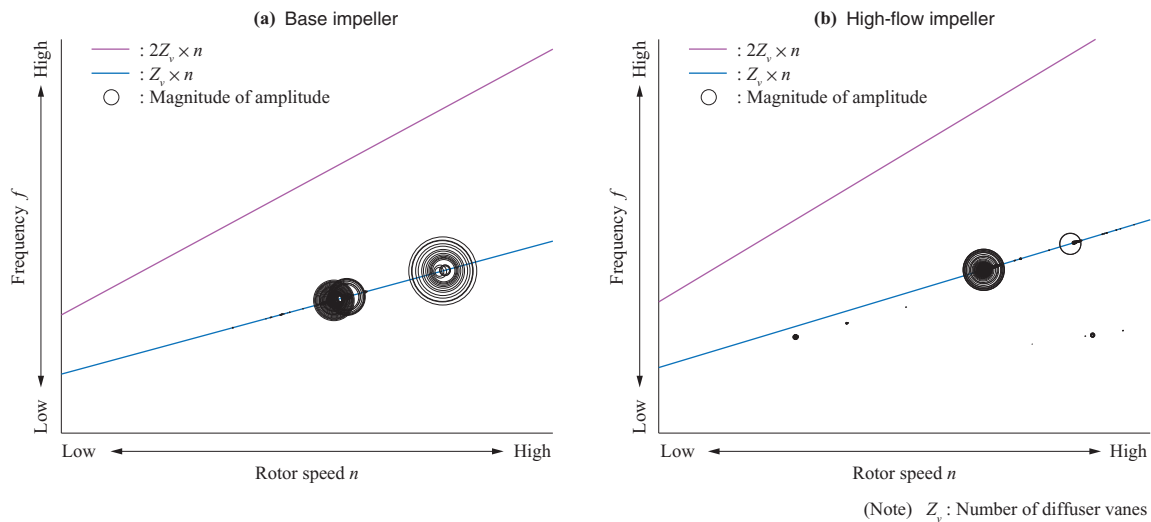


Fig. 15 Measurement results for an evaluation of the impeller blade's vibration response

impeller as well, the peak response is observed at diffuser excitation order. However, the response is considerably low. In addition, although the increase in exciting force associated with the thickening of the diffuser vanes was a concern, the optimization design of the impeller blade thickness allowed the stiffness of the impeller to be increased, and therefore a lower response could be obtained even though the flow capacity of the impeller was increased.

6. Conclusion

In the development of a turbo-compressor aiming at an increase in flow capacity exceeding a conventional level, a highly reliable high-flow compressor exhibiting high performance could be developed by appropriately combining the CFD analysis, FEM analysis, and optimization approach.

The compressor stage described in this report has already been applied to some turbo-compressors, and is contributing to performance and reliability improvement and to cost reduction.

REFERENCES

- (1) M. Matsukuma : Air Compressor (Energy-Saving Technology Practice Series) The Energy Conservation Center, Japan (2005) p. 30
- (2) C. Rodgers : The Efficiencies of Single-Stage Centrifugal Compressors for Aircraft Applications ASME Paper 91-GT-77 (1991)
- (3) H. Kure, H. Mori and O. Watanabe : Study on Methodology for Total Design Management IHI Engineering Review Vol. 43 No. 2 (2010) pp. 77-88